Electronic Supplementary Material (ESI) for Soft Matter.

Crack morphologies in drying suspension drops

Electronic Supplementary Information

Philippe Bourrianne*, Paul Lilin, Guillaume Sintès, Traian Nîrca, Gareth H. McKinley, and Irmgard Bischofberger*

Department of Mechanical Engineering, Massachusetts Institute of Technology
77 Massachusetts Avenue, Cambridge, MA 02139, USA
* philippe.bourrianne@princeton.edu, *irmgard@mit.edu

Supplementary Movies

MovieS1: Side view of a 2 μL drop of Ludox suspension with initial volume fraction ϕ = 22% deposited on a glass slide. The movie is accelerated 20 times. The drop spreads on the hydrophilic glass slide and adopts a spherical cap shape of volume $\Omega = \pi {R_0}^3 \sin\theta\,/4$ with a contact angle θ = 20° and a contact radius R_0 = 1.5 mm. During drying, a spherical liquid cap recedes on top of the particle deposit. The deposit bends into a convex structure.

MovieS2: Bottom view of an 0.3 μL drop of Ludox suspension with ϕ = 22% in the single-crack regime, imaged on an inverted microscope in transmission mode. The spherical liquid cap recedes on top of the particle deposit. Radial cracks in the deposit propagate by avalanches leading to the formation of regularly spaced petals. The movie is accelerated 10 times.

MovieS3: Bottom view of an 0.3 μL drop of Ludox suspension with ϕ = 1.7% in the double-crack regime, imaged on an inverted microscope in transmission mode. Radial cracks in the outer part of the deposit propagate by avalanches. At a distance ∼150 μm from the drop edge, the cracks branch into secondary cracks. The movie is accelerated 10 times.

MovieS4: Bottom view of an 0.3 μL drop of Ludox suspension with ϕ = 0.75% in the ring-crack regime, imaged on an inverted microscope in transmission mode. Radial cracks in the deposit propagate by avalanches. The particle deposition is limited to a ring at the periphery of the drop. The movie is accelerated 10 times.

MovieS5: High-speed movie of an 0.5 μL drop of Ludox suspension with ϕ = 22% in the single-crack regime using an interfero-microscopy setup. Cracks started to form prior to the beginning of the movie. The interference fringes reveal a lateral delamination of the petals from the substrate. This delamination process is a precursor for the formation of a subsequent neighboring crack. The movie is slowed down 50 times.

Influence of the initial drop contact angle on the crack regimes

We probe the sensitivity of the crack patterns to a change in the initial drop contact angle using a silanized glass slide coated with 3-glycidyloxypropyl-trimethoxysilane (TCI). The contact angle is $\theta = 40 \pm 2°$, larger than the contact angle $\theta = 20 \pm 3°$ in our other experiments. We deposit 1 µL drops of Ludox suspensions of different volume fractions ϕ in a controlled environment with relative humidity $RH = 50 \pm 2\%$. We observe the same regimes of ring cracks, double cracks and single cracks, as shown in Fig. S1, indicating that these regimes are robust to changes in the initial contact angle in the range of $20° < \theta < 40°$.

A further increase of the contact angle, however, will affect these regimes. The occurrence and number of cracks then depends on whether the contact line stays pinned or slips on the substrate as the drop dries. Slippery substrates with contact angles close to 90° can lead to a suppression of the cracks[1,2]. On superhydrophobic substrates, the drop adopts a quasi-spherical shape and a solid crust of concentrated particles forms at the drop surface, which buckles under capillary pressure prior to crack formation[3–5].

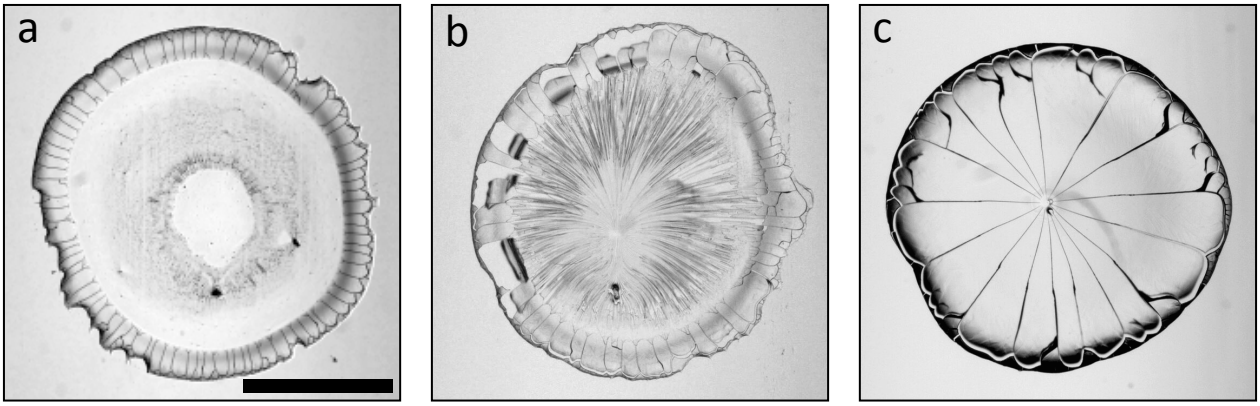

Figure S1: Crack patterns obtained for 1 µL drops of Ludox suspensions for an initial drop contact angle $\theta = 40 \pm 2°$. (a) Ring cracks for ϕ = 0.67%, (b) double cracks for ϕ = 1.12%, and (c) single cracks for ϕ = 13.5%. The scale bar represents 1 mm.

Sensitivity of crack regimes to particle type

To probe for the sensitivity of the observed crack regimes to the type of particles used, we perform experiments using carboxylated polystyrene beads (PS) (CA040NM, Magsphere) of diameter 44 nm. The particles are of comparable size to the silica (Si) Ludox particles of diameter 22 nm, but their shear modulus is more than a factor of ten smaller (1.6 GPa $= G_{PS} \ll G_{Si} =$ 31 GPa)[6,7]. We deposit 0.3 µL drops of polystyrene suspensions of different particle volume fractions ϕ on a clean glass slide in a controlled environment with relative humidity $RH = 54\%$. Remarkably, we observe the same regimes of ring cracks, double cracks and single cracks for polystyrene suspensions as those observed for Ludox suspensions, as shown in Fig. S2. It is interesting to note that while the same crack regimes are observed for the two types of particles, the characteristics of the cracks depend on the particle type. The deposits formed from polystyrene suspensions exhibit additional orthoradial cracks and a more limited delamination.

Larger changes in the particle hardness, however, are known affect the cracking behavior[7]. For suspensions of very soft polymer particles, the deposit wrinkles but does not crack, as the capillary pressure can deform the particles without inducing a crack[8].

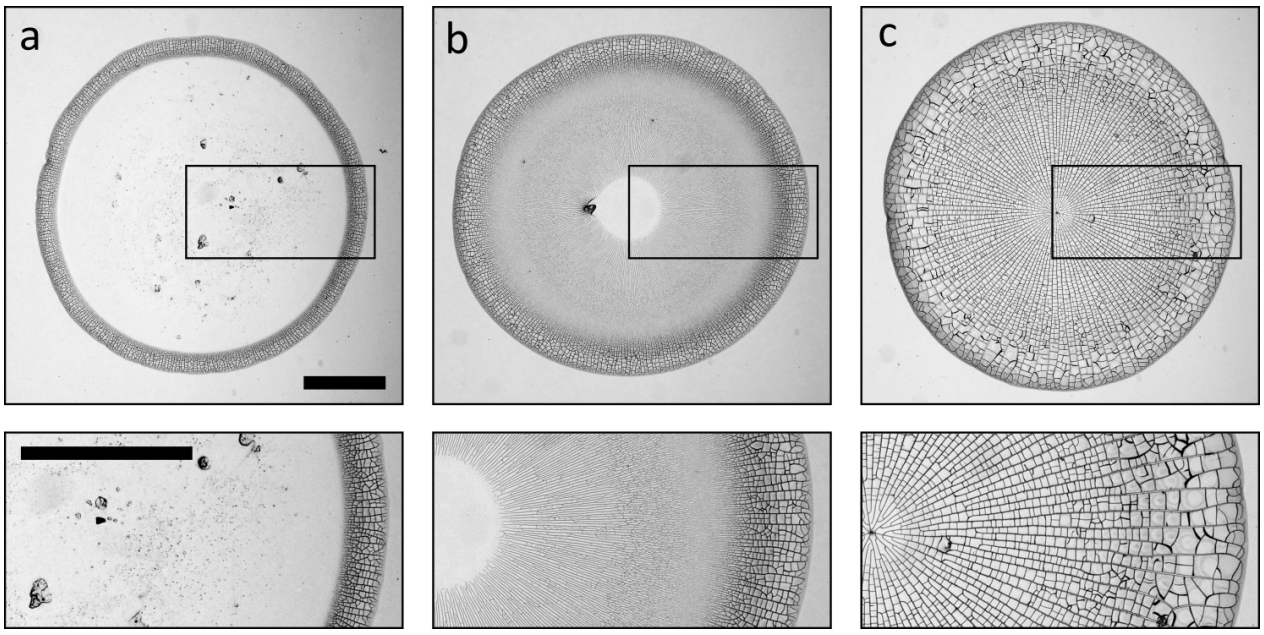

Figure S2: Cracks patterns for 0.3 µL drops of suspensions of carboxylated polystyrene particles with diameter of 44 nm. The same crack regimes occurring for Ludox suspensions are observed for polystyrene suspensions: (a) Ring cracks for ϕ = 1%, (b) double cracks for ϕ = 3%, and (c) single cracks for ϕ = 10%. The bottom images show zoomed views. The scale bars represent 500 µm.

Influence of the initial volume fraction on the number of cracks in the single-crack regime

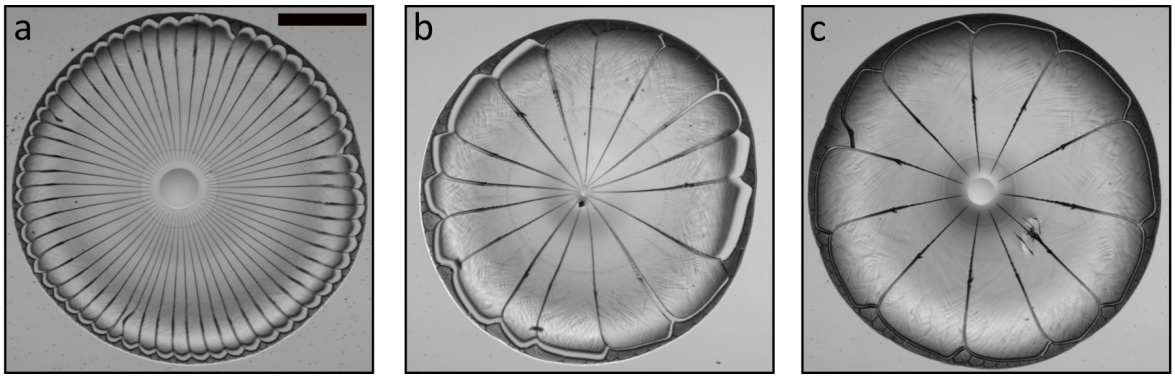

Figure S3: Crack patterns for 0.3 µL drops in the single-crack regime. The number of cracks decreases as the initial particle volume fraction increases from (a) ϕ = 8.4%, (b) ϕ = 15% to (c) ϕ = 22%. The scale bar represents 500 µm.

Relation between crack spacing and deposit thickness

We measure the maximum thickness h of the deposit and the spacing d_c between cracks of a given drop using a laser scanning confocal microscope (VK-X 3D, Keyence). The distance between cracks is measured at the perimeter of the drop, as shown in the inset of Fig. S4). It increases monotonically with the deposit thickness, in fair agreement with a linear relationship $d_c \propto h$ suggested in previous studies[2,9,10], as displayed in Fig. S4.

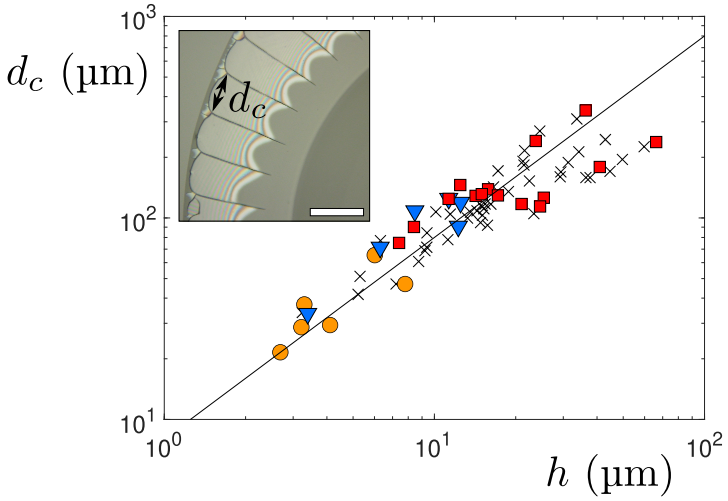

Figure S4: The crack spacing d_c versus the deposit thickness h. The crack spacing at the perimeter of the drop and the maximum thickness are measured for drops in the ring-crack regime (orange circles), double-crack regime (blue triangle) and single-crack regime (red squares). As the profilometry measurement is only possible before cracks start to form, the exact crack regime can not always be determined; for those drops where the crack regime is unknown, we report the data as black crosses. The solid line denotes a linear relationship suggested in previous studies[2,9,10]. Inset: Definition of the crack spacing d_c for an 0.3 µL drop with particle volume fraction $\phi = 12\%$. The scale bar represents 150 µm.

Influence of drying dynamics on crack pattern

To probe the influence of the drying time on the crack characteristics and the number of cracks, we perform two additional sets of experiments:
(i) We use different drop volumes, ranging from 0.3µL to 5µL. This allows us to change the drying time τ_d by a factor of ~6. Both the ratio w/R_0 of the crack length w to the initial drop radius R_0 and the number of cracks N_c remain unchanged for different drop volumes, as shown in Fig. S5a,c.
(ii) We vary the relative humidity RH in our experimental chamber. We use saturated solutions of sodium chloride to reach $RH = 48\% \pm 4\%$ and saturated solutions of potassium sulfate to reach $RH = 67\% \pm 4\%$. The drying time τ_d changes by a factor of six for a change in relative humidity from 15% to 75%. A change in the relative humidity does not affect the ratio of the crack length w to the initial drop radius R_0, nor the number of cracks, as shown in Fig. S5b,d.
The drying time τ_d is thus not a control parameter for the crack morphology within the range of drying times investigated. This observation is in apparent contradiction with recent studies[11,12], but could be due to the relatively small size of our droplets which always leads to fairly fast drying dynamics.

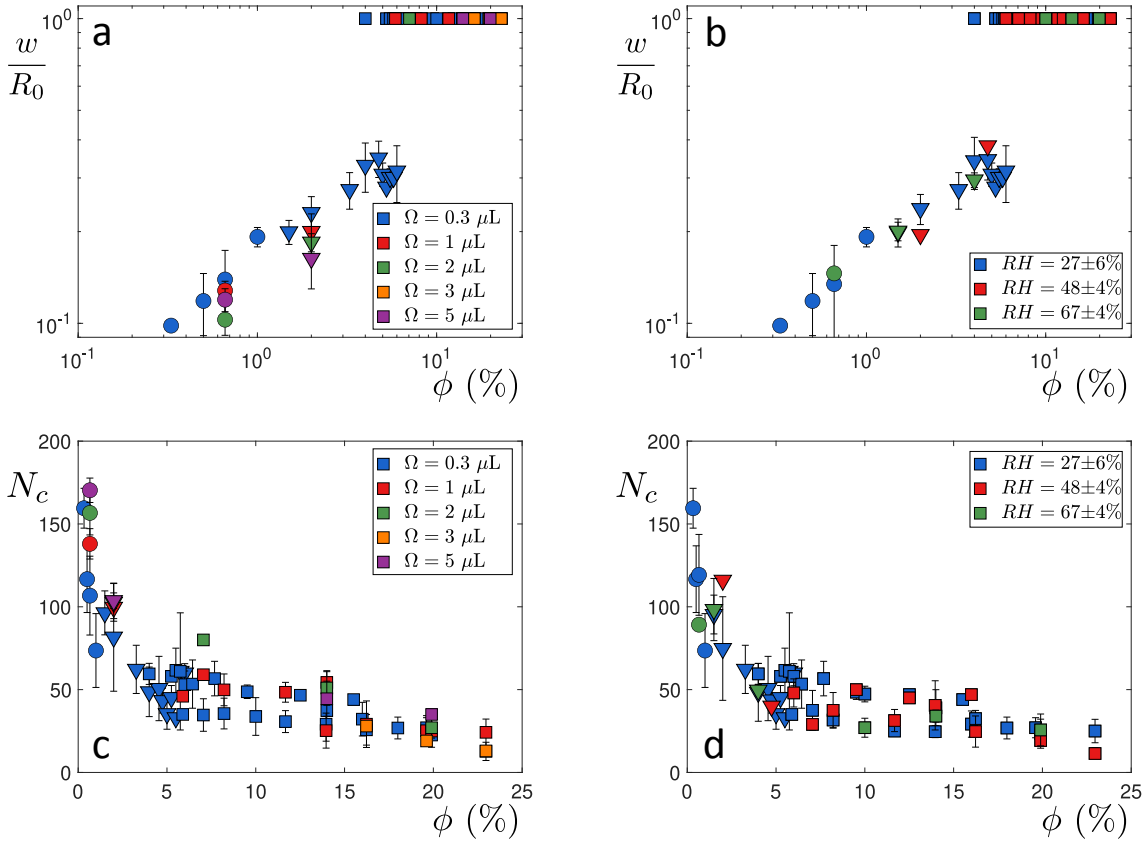

Figure S5: Influence of drop volume and relative humidity on the crack patterns. (a,b) Normalized width of the pattern w/R_0 and (c,d) number of cracks N_c versus initial volume fraction ϕ for drops of different volumes Ω in controlled environments of different relative humidities RH. Circles denote the ring-crack regime, triangles the double-crack regime and squares the single-crack regime. The data are obtained with Ludox particles of diameter 22 nm.

The independence of the number of cracks N_c on the drop volume observed in Fig. S5 can be understood by considering that both the deposit height and the drop perimeter $2\pi R_0$ increase with drop volume as $h \propto \Omega^{1/3}$ and $R_0 \propto \Omega^{1/3}$. Considering that the crack spacing $d_c = (2\pi/N_c)R_0$ increases linearly with the deposit thickness, we indeed do not expect a change in the number of cracks with drop volume.

Influence of the substrate temperature T on the maximum deposit thickness h

We perform thickness measurements on a laser confocal microscope (VK-X 3D, Keyence) at ambient temperature T = 20°C and also at T = 15°C using a Peltier plate to cool the substrate. The maximum deposit thickness h is independent of the substrate temperature T within the temperature range investigated, as shown in Fig. S6a. Likewise, the deposit thickness h is independent of relative humidity RH within the range from $18 \pm 8\% \leq RH \leq 71 \pm 2\%$, as shown in Fig. S6b. These observations are in agreement with the independence of the crack morphology and the number of cracks on drying time.

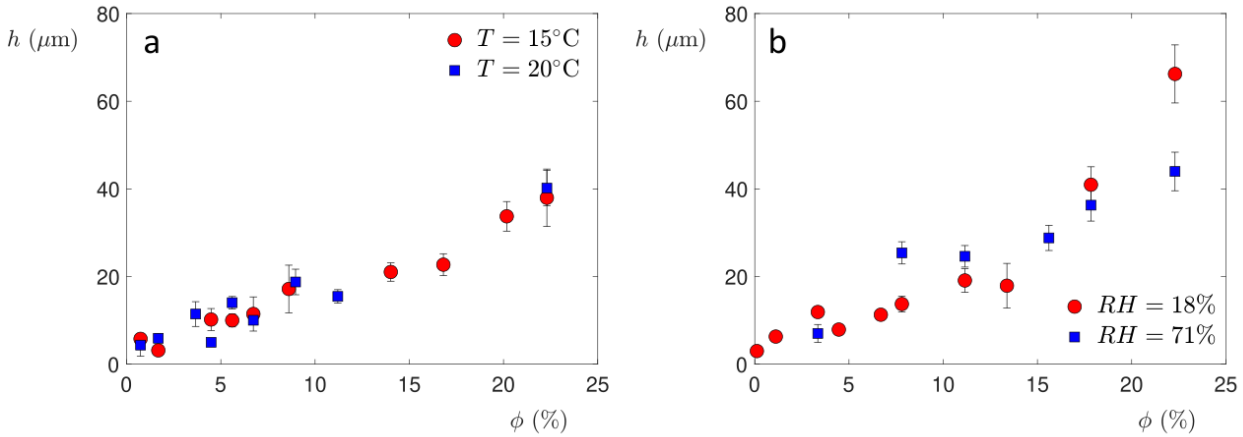

Figure S6: The maximum deposit thickness h is independent of (a) the substrate temperature for T = 15°C and T = 20°C and (b) the relative humidity RH within the range from $18 \pm 8\% \leq RH \leq 71 \pm 2\%$.

References

1 U. U. Ghosh, M. Chakraborty, A. B. Bhandari, S. Chakraborty and S. DasGupta, *Langmuir*, 2015, **31**, 6001–6010.

2 N. Yan, H. Luo, H. Yu, Y. Liu and G. Jing, *Colloids Surf. A: Physicochem. Eng. Asp.*, 2021, **624**, 126780.

3 L. Pauchard and Y. Couder, *Europhys. Lett.*, 2004, **66**, 667–673.

4 S. Basu, L. Bansal and A. Miglani, *Soft Matter*, 2016, **12**, 4896–4902.

5 I. B. Dogru, C. Kosak Soz, D. A. Press, R. Melikov, E. Begar, D. Conkar, E. N. Firat Karalar, E. Yilgor, I. Yilgor and S. Nizamoglu, *Mater. Chem. Front.*, 2017, **1**, 2360–2367.

6 R. C. Chiu, T. J. Garino and M. J. Cima, *J Am. Ceram. Soc.*, 1993, **76**, 2257–2264.

7 K. B. Singh and M. S. Tirumkudulu, *Phys. Rev. Lett.*, 2007, **98**, 218302.

8 H. M. van der Kooij, G. T. van de Kerkhof and J. Sprakel, *Soft Matter*, 2016, **12**, 2858–2867.

9 K. A. Shorlin, J. R. de Bruyn, M. Graham and S. W. Morris, *Phys. Rev. E*, 2000, **61**, 6950–6957.

10 V. Lazarus and L. Pauchard, *Soft Matter*, 2011, **7**, 2552.

11 W. Bou Zeid and D. Brutin, *Colloids Surf. A: Physicochem. Eng. Asp.*, 2013, **430**, 1–7.

12 F. Giorgiutti-Dauphiné and L. Pauchard, *Eur. Phys. J. E*, 2014, **37**, 39.